Classical and Quantum Scattering

J. Woudenberg

April 29, 2011

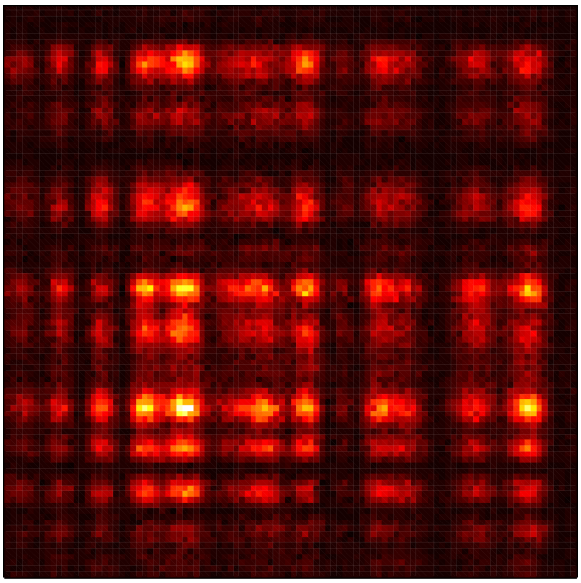

Quantum Optics and Quantum Information group
This project was supervised by:
Drs. H. Di Lorenzo Pires
Dr. M.P. van Exter

Contents

Introduction

This master thesis describes the research I did during my master project in the Quantum Optics group at the University of Leiden. For a number of practical reasons I have been involved with 3 different experiments, though these experiments are very much related to one-another. In this introduction I will present a short overview of these experiments and explain how they came about.

Chapter 1 deals with the enhanced backscattering project I have worked on. Enhanced backscattering is an effect observed when light is reflected from a scattering random medium. A peak in the backward direction, the direction opposite to the incident light, is observed. The phenomenon has been studied extensively over the past years, but a version of the experiment using entangled photons as a light-source has never been performed.

Our goal was to attempt first the standard classical version of the experiment, to get a feel for the experimental difficulties we would have to face in the two-photon version. After we had done this, we decided to postpone the two-photon version of the experiment, primarily because an existing setup that would need to be heavily modified for this new experiment could, with only minor modifications, also be used to perform another experiment first (the one discussed in Chapter 3).

Chapter 2 is about symmetries in two-photon scattering. When entangled photons are sent through a scattering medium, they are more likely to end up on top of each other than apart. This is a result of the bosonic nature of photons. However, by changing the symmetry of the input field, we can simulate fermionic and so called anyonic behaviour as well. Wouter Peeters had already performed extensive measurement on the bosonic and fermionic behaviour [5]. I performed measurements for the anyonic case.

It is interesting to note that this experiment is the forward scattering analogue of the planned two-photon backscattering experiment I described before. Therefore the results of this experiment heavily influenced our predictions of what we would see in the backscattering case (two-photon bunching). On a practical level too, the through-scattering experiment suggested solutions to experimental problems in the backscattering experiment (simulating a random media using a phase plate).

Chapter 3 describes the last experiment I performed, on speckle statistics at a reduced number of modes. This experiment was inspired by a paper from Beenakker et al. [6]. We took the setup with the volume scatterer from Chapter 2, and altered it to produce the fewest

amount of entangled input modes possible. In this regime, contrary to the many-mode regime we were in before we changed the setup, we also observe one-photon speckle. Our two-photon speckle pattern now reduces to the product of two one-photon speckle patterns.

In order to analyse these speckle patterns statistically we wrote a new measuring routine. After analysing we found out that our results necessitated a more general theory than the one in the Beenakker paper. This new theory fits our experimental data quite well.

1 One-photon Enhanced Backscattering

1.1 Introduction

Enhanced backscattering in random media is an effect that has been known for quite some time now. It results from the fact that when a scattered ray exits a random media under the same angle that it entered, its path through the medium has a time-reversed twin that it interferes with constructively. As a result the measured intensity of the scattered light in the backward direction is twice the intensity it is for other directions.[1]

The angular profile of the reflected light is expected to be uniform, except in the backscatter-direction where a cone of a factor two is visible. The shape of this cone is found to be [3]

$$a(q) = \frac{1}{2}\frac{3}{8\pi}\left[1 + 2\frac{z_0}{l^*} + \frac{1}{(1+ql^*)^2}\left(1 + \frac{1-e^{-2qz_0}}{ql^*}\right)\right] \tag{1}$$

Here z_0 is penetration depth of the light, l^* is the mean free path and $q = 2\pi\theta/\lambda$, where θ is the angle over which the light is scattered back and λ the wavelength. We can simplify this equation by replacing the exponential with a first order approximation and normalizing the background level to 1. Then we find

$$I = 1 + \frac{1}{(1+c|\theta|)^2} \tag{2}$$

Here $c = 2\pi l^*/\lambda$. This result gives an intensity of 2 if $\theta = 0$ and drops to 1 when $|\theta|$ becomes larger. The backscatter cone can be imaged using a detector on a rotating arm [2] but also by making a far-field image of the sample using a CCD. We performed this simpler version of the experiment as an introduction to a more complex version with a two-photon light-source. This latter version has not yet been attempted.

1.2 Experiment

Because this was an introductory experiment the setup changed a great deal as we tried to optimize it. Figure 1 shows the final version of the setup, which was also used to perform the measurements resulting in Figures 2 and 3.

In the input arm, a lens collimates the 826nm diode laser light coming from a fiber. The light moves through some optical components and onto a scattering medium - we used paper and white paint - which can be rotated to average speckle.Lens 1 ($f = 25mm$) focuses the laser light coming from the fiber. Lens 2 ($f = 6mm$) creates a far-field image of the back-reflected light in its focal plane, and this plane in turn is imaged by lens 3 $f = 6cm$ onto the CCD with some suitable magnification (for the final paint measurements, this was $2/3\times$, the distance from the back focal plane of lens 2 to lens 3 was $15cm$, the distance from lens 3 to the CCD was $10cm$). Single-scattering

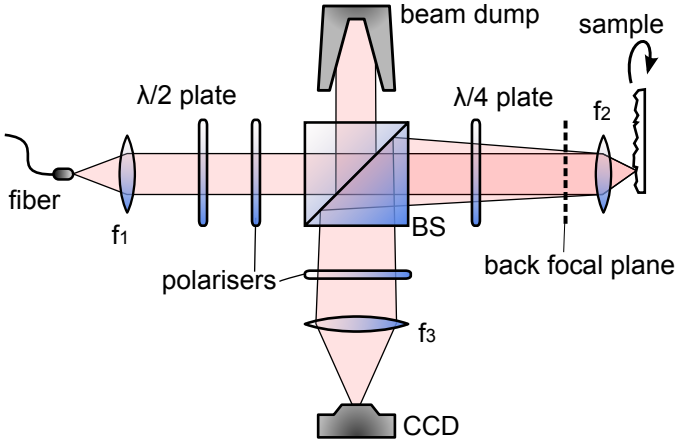

Figure 1: Setup of the enhanced backscattering experiment.

events do not contribute to the enhanced-backscattering cone. To get rid of them we use the technique outlined in the paper by Muskens et al. [2]; the polarisers combined with the $\lambda/4$ plate select the helicity conserving EBS-light. Lastly, because light coming from the fiber is in general polarized to some degree, we use the $\lambda/2$ plate to rotate this polarization to best match the the transmission axis of the first polariser.

The biggest experimental difficulties we encountered all had to do with the stray light. Because the light incident on the scattering medium is scattered over all possible angles you only recollect a small part of the light and the setup is very sensitive to stray light.

One recurring problem was that any of the components in the sample-arm of the setup directly reflected some of the incident light. These reflected coherent beams, though weak, can look very similar to a backscatter cone on the CCD. We could also see the internal reflection of the beam splitter. To deal with this problem, the $\lambda/4$ plate, the sample, and the beam splitter were placed under an angle. Rotating the beam splitter did not only affect the internally reflected light, but the back-reflected light as well, albeit in a different way, so the CCD-arm of the setup needed to be placed under an angle as well.

We also tried to collect as much of the light as possible, by putting a strong lens close to the sample. The disadvantage of this approach is that the beam incident on the sample won't be collimated. Because the incident light doesn't have a single direction, the backscattered light will effectively consist of a mixture of backscatter-cones. We will still observe a cone, but its sharp peak will be degraded. It is possible to compensate for this somewhat by moving a lens directly behind the fiber, pre-focussing the beam in such a way that after the second lens, the light is as collimated as possible.

Another form of stray light is simply background light. This could be

dealt with pretty effectively by putting a color filter in front of our CCD, and also by performing dark measurements and by subtracting those from our data.

1.3 Results

Figure 2 shows a CCD image of a typical backscatter cone. In this case a paint sample (TiO_2) was used.

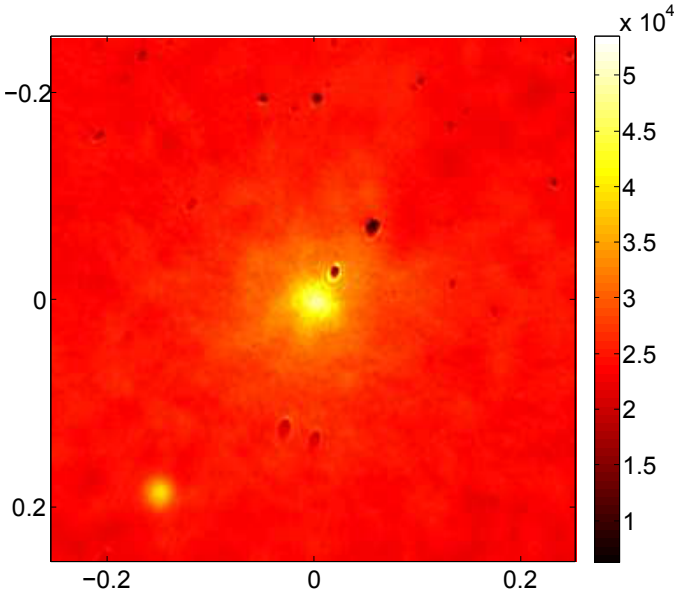

Figure 2: A CCD picture of an enhanced backscattering cone.

By rotationally averaging this image we get Figure 3. The cone-shape is clearly visible and we can also confirm that its peak is a factor two higher than the background signal. It has been fitted with equation 2.

For c in equation 2, a measure of the width of the peak, we find a value of 17. From this we can calculate the mean free path of the scattered light l^* and find it to be $2.3\mu m$.

1.4 Discussion

In conclusion, we completed a classical enhanced backscattering experiment. The things we have learned will be useful when a complex version of the experiment is performed with a two-photon source. From this experiment, and also calculations that have been performed on the side, it seems that the low intensity you expect to get from the back-reflected light will be the biggest problem in this new experiment.

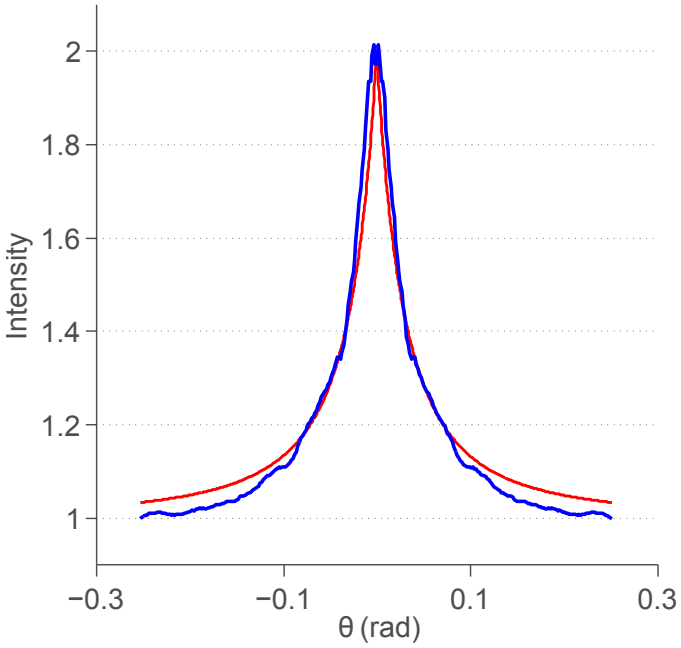

Figure 3: A cross-section of an enhanced backscattering cone (blue), fitted with equation 2 (red).

One possibility to partially overcome the obstacle of low signal strength (in our final setup roughly one percent of the laser power reaches the CCD), is to simulate a random medium using a diffuser plate and a mirror [4]. such a simulated medium would scatter the light only over a limited scattering angle, thus allowing more light to be collected.

2 Symmetries in two-photon scattering

2.1 Introduction

When we send entangled photons through a scattering medium and measure their positions on the other end, there is a relatively large likelihood of finding the two scattered photons at the same position. This is a result of the bosonic symmetry of these photons. We can modify this symmetry to get fermionic or anyonic behaviour.

My contribution to this topic deals mainly with measurements on the anyonic behaviour, and builds heavily on the work done by Wouter Peeters, culminating in his thesis [5]. Furthermore, M.P. Exter is writing a paper on the subject, a recent version of which is included in appendix A.

2.2 Experiment

Figure 4 shows the setup used for this experiment. A 413nm pump laser is focused inside a type-II PPKTP crystal. This generates red (826nm) photon-pairs, with orthogonal polarizations. The pump light is blocked out, and the photon-pairs, henceforth referred to as SPDC-light, go through an f-2f-f configuration, in the center of which a wave plate can be placed.

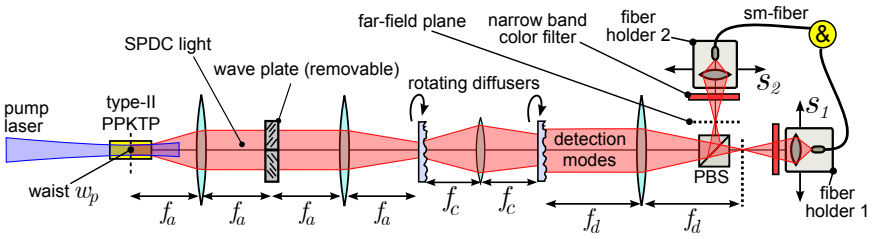

Figure 4: Setup of the bunching experiment. Modified image from Wouter Peeters' thesis [5]

The light then goes through the volume scatterer. We simulate a volume scatterer using two diffusers in an f-f configuration. This way we are sure both the near and far-field of the SPDC light is randomized. By using such a 'simulation' instead of a real volume scatterer we can keep the angles over which the light is scattered under control, and keep most of the light in the setup. Both diffusers can be rotated to average out speckle.

A polarizing beamsplitter splits up the photon-pairs. Using two detectors coupled with coincidence circuitry, the pairs are then counted. The detectors are looking at a far-field image of the second diffuser.

Without any phase-plate we observe bosonic behaviour in the two-photon coincidences (see below). We can also add a dual retarder plate to introduce a total $\phi/2$ or $\phi/4$ phase difference between both photons; this results in

respectively fermionic and anyonic behaviour (see appendix A). This dual retarder plate consists of two halves. When placed exactly in the centre of the beam, most of the time two photons belonging to a pair will go through opposite halves. The dual retarder plate can be centred relatively easy by sending a (partially blocked) pump through it, and watching the plate from the side using a simple camera. When the pump beam hits the centre of the plate, where both halves meet, light is scattered in every direction. Watching the scattered light with the camera we move the plate sideways, and note the positions where the scattered light disappears. The desired centre location is in between these two positions.

Some time is spend aligning both detectors. When both are centred, they should look at the same spot in both the near and far-field. To help with the alignment, a diode laser can be shot back through the detecting single-mode fibers. Two cameras, positioned in the near and far-field plane of the detectors, allow us to directly see the detection modes of both detectors. Each detector has six degrees of freedom: The entire stage can be moved, which moves the detection mode in the near but not the far-field. Also, the fiber tip can be moved separately, leaving the lens in front of it in place. This will affect the detection modes in both the near and far-field. The best alignment-strategy then is to first put both detection modes on top of each other in the far-field, using the fibre actuators, and then do the same in the near-field using the stage actuators (which will keep your far-field alignment intact).

2.3 Results

In figure 5, results for bosonic and fermionic behaviour are shown. It is clear that in the bosonic case, the photons bunch together on the diagonal (both detectors are looking at the same coördinate), whereas in the fermionic case we observe anti-bunching. The centre image shows cross-sections obtained by projecting on an axis orthogonal to the (anti)bunching diagonal. For this projection, only points lying within a 45 degree rotated rectangle are included.

Figure 6 shows the anyonic case. We see both a bright and a dark line along the diagonal, and in fact the order of these lines can be switched by turning around the dual retarder plate.

Figure 7 shows cross-sections for both orientations of the dual retarder plate (black and blue curves). So far all scans have involved detectors moving over ranges that lie in the plane of the optics table. When we performed an anyonic measurement by scanning a vertical range we got a completely different result (red curve), showing no structure at all. We believe this has something to do with the fact that the dual retarder plate has an orientation of its own, the line that separates both halves of the plate. In the first measurements we scanned orthogonal to this line, in the last measurement

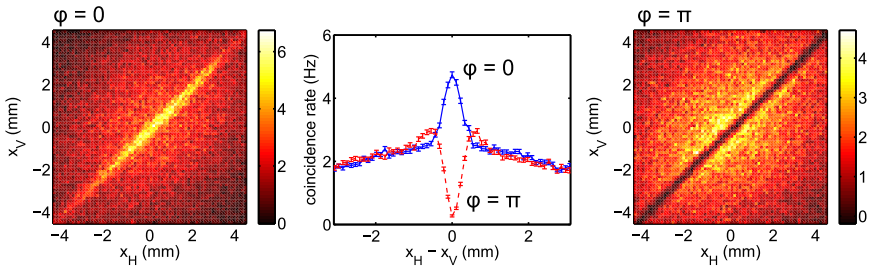

Figure 5: Two-photon coincidence figures of bosonic and fermionic behaviour. The left figure shows a false color plot of the coincidence count rate $R_{cc}(x_1, x_2)$ as a function of both detector (stage) positions for the bosonic case. The right figure is the fermionic equivalent. The center figure shows averaged cross-sections for both measurements, obtained by projecting along the $x = y$ diagonal.

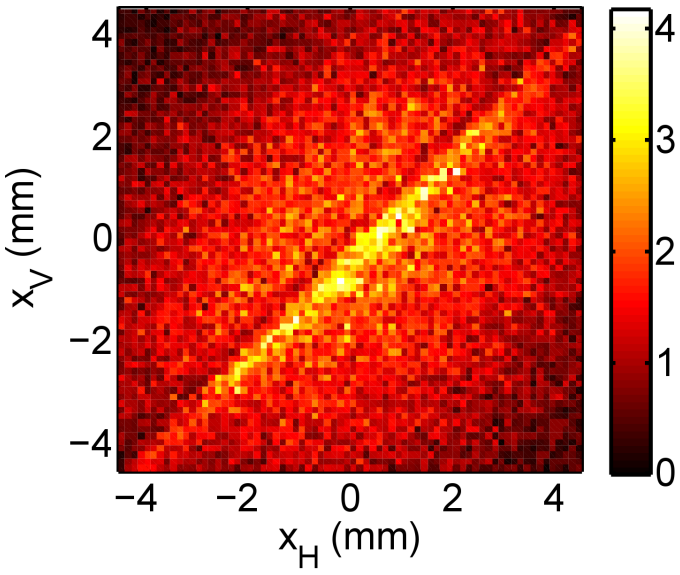

Figure 6: The anyonic equivalent of the false-colour plots in figure 5.

we scanned parallel to it. We currently think that the last measurement is the most 'natural' shape of the anyonic behaviour, while the wiggle we see in the first scans is an artefact resulting from our specific setup, associated with the fact that the scattering angle of the diffuser plates is comparable to the opening angle of the incident SPDC light.

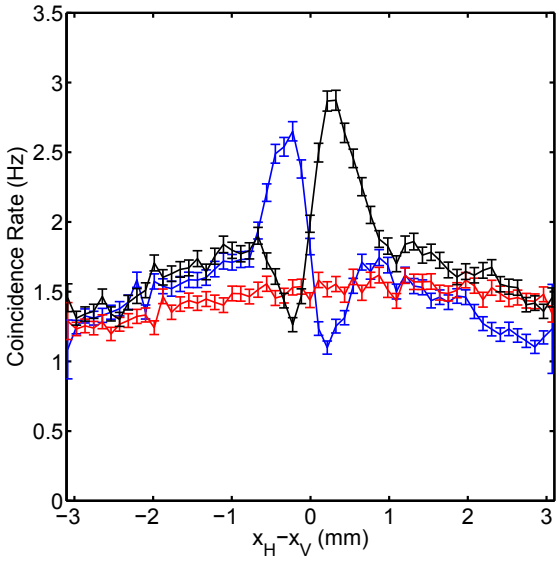

Figure 7: Cross-sections similar to the ones found in figure 5, for three different anyonic measurements. For the black and blue curves, both detectors scanned a range orthogonal to the orientation of the dual retarder plate (x_1-x_2), for the red curve we scanned along the plane (y_1-y_2).

2.4 Discussion

We have seen that by adding a dual retarder plate into our setup we can modify our two-photon field to show fermionic or anyonic behaviour, instead of the bosonic behaviour we naturally expect from photons.

3 Two-photon scattering at a reduced number of modes

3.1 Introduction

The setup we used for the measurements in the previous chapter produced a relatively large amount of modes. The Schmidt number, a measure of the amount of entangles spatial modes, was about 83 for those measurements[5]. For the last part of my master project, I was aiming for the opposite, measurements at reduced mode or Schmidt number K. Specifically we were interested in testing experimentally the theoretical paper on this subject by Beenakker et al. [6]. The key results of this paper are the probability distributions of coincidences, depicted in figure 8.

H. Di Lorenzo Pires is writing a paper on the subject, a recent version of which is included in appendix A.

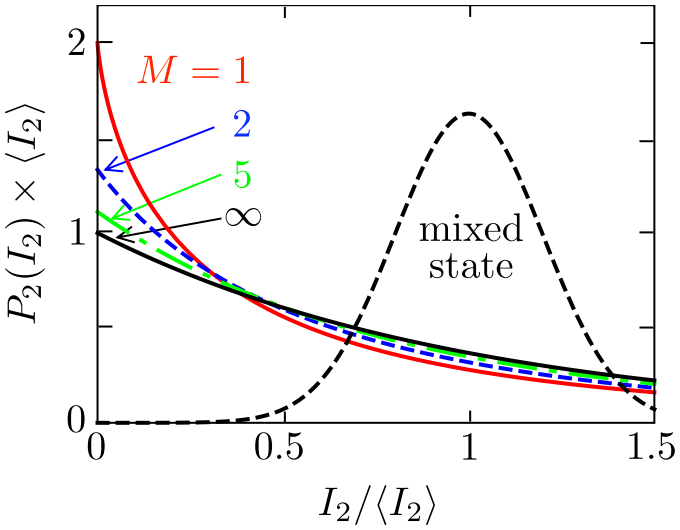

Figure 8: Theoretical predictions of the intensity distributions of two-photon speckle patterns for pure states (figure copied from a paper by Beenakker et al. [6]). In this paper, I_{cc} is referred to as I_2. Furthermore, modes are counted in a different way; Our mode number $K = 2M$.

3.2 Experiment

To minimize the amount of modes our setup produced we use the results in the paper by Law and Eberly [7], who offer a way to calculate the Schmidt number as a function of the crystal length and the Raileigh length of the focused pump laser. We obtained a measured Schmidt number of $K = 1.5$

by using a $5mm$ PPKTP crystal and focussing the pump enough to produce a $11\mu m$ waist.

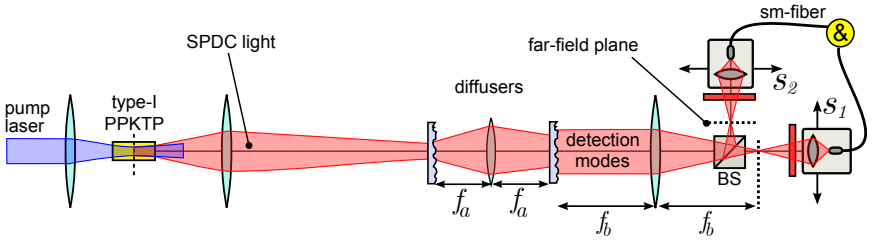

Figure 9: The setup used to make the reduced mode measurements.

Our new setup is shown in figure 9. To build it, only minor changes with regards to the previous setup depicted in figure 4 were needed. The pump beam is now focussed quite strongly in the crystal using a $f = 10cm$ lens. Furthermore we swapped our type-II PPKTP crystal for a type-I, because this provides more SPDC light. As a result of this change, the polarizing beamsplitter was also replaced with a non-polarizing one. Last we would like to keep the SPDC spot size on the first diffuser roughly the size it used to be ($140\mu m$), which would allow us to keep the detection part of the setup the same too. Therefore we replaced the f-2f-f lens configuration by a single lens that makes a roughly $10\times$ magnified image of the SPDC source on the first diffuser. As a result of these changes, and in particular the switch to a type-I crystal, we have dramatically increased the detected coincidence rate.

We had some trouble with aligning the diffusers. While rotating them, the measured counts per second would oscillate at a frequency correlated to the angular speed of the diffusers. We realized this was probably due to the diffusers being mounted under a small angle with regards to the optical axis. By careful adjustments we managed to minimize this effect.

3.3 Results

A two-dimensional two-photon speckle pattern for a small amount of modes can be seen in figure 10. The grid-like shape of the speckle pattern shows us that it is simply the product of two one-photon speckle patterns, one for each detector. This is quite the opposite of what we observe when we have more modes; in that case we observe only two-photon speckle in a seemingly random two-dimensional pattern, but no one-photon speckle.

In order to analyse these speckle patterns we changed our measurement procedure somewhat. Instead of letting both detectors scan together we fix both of them in place, either on top of each other or at separate locations. We then perform a measurement of typically $5s$, rotate the diffusers enough (about $3°$) to present the detectors with another realization of the scatter-

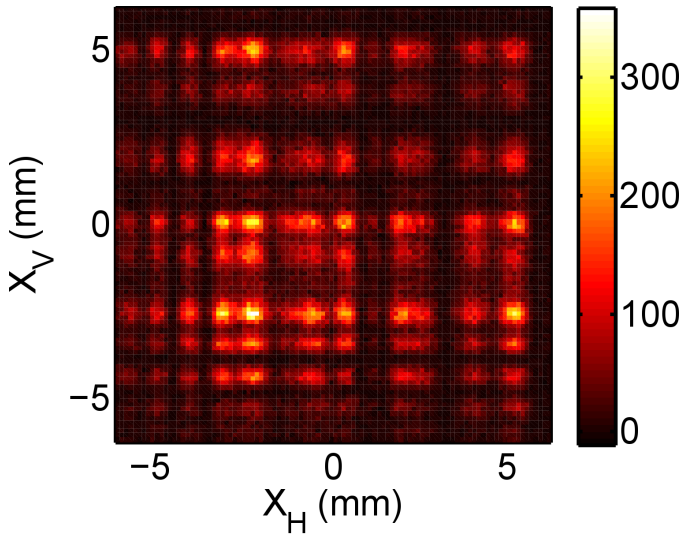

Figure 10: A false colour plot of the coincidence count rate as a function of both detector positions showing a low-mode speckle pattern.

ing medium, measure again, rotate, etc. With 2 diffusers, this gives us a maximum of $(360/3)^2 = 14400$ unique measurements.

A small interval in a longer measurements series is presented in figure 11. The counts of one detector are shown. Similar data is generated by the other detector and the coincidence circuitry.

Figure 12 and 13 present the probability distributions of the measured coincidence counts.

It is tempting to compare the height of the peak in this figure with results from the Beenakker paper as seen in figure 8, but this peak can be heightened or lowered by changing the binning size of the histogram, and should thus be approached with some scepticism. What we can learn from the experimental figures is that our speckle patterns without any doubt exhibit non-exponential statistics. Furthermore, we see a difference between the $x_1 = x_2$ and the $x_1 \neq x_2$ case.

The Beenakker paper only considers the $x_1 \neq x_2$ case and these results show that we need a more general theory. Another limitation of the Beenakker theory is that it assumes discrete values for the mode number $M = 1, 2, ...$ which translates to $K = 2, 4, ...$ We work with a mode number $K = 1.5$, which is both lower than $M = 1$ and not discrete. Martin van Exter worked on a theory that generalizes Beenakkers theory, the result of which is summarized in the following equations. Equation 4 is a generalization of Beenakkers theory, equation 5 is new.

$$\mathcal{V}_1 = \frac{1}{K} \tag{3}$$

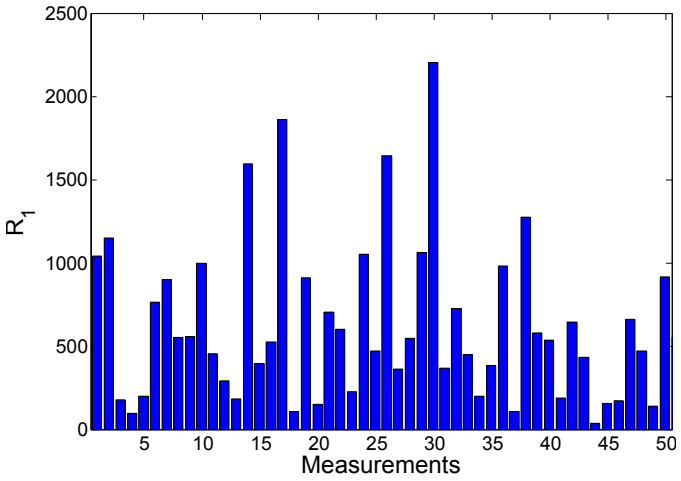

Figure 11: 50 datapoints out of a 13699 datapoint measurement, showing single-detector counts at consecutive diffuser settings.

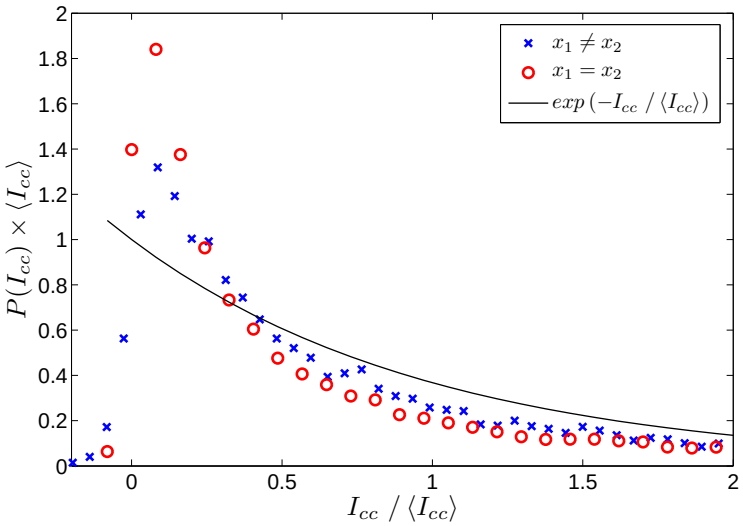

Figure 12: Probability distributions like the ones in figure 8. These were obtained from measurements of the coincidence count rates for detector positions $x_1 = x_2$ and $x_1 \neq x_2$. A normalized exponential curve has been plotted alongside.

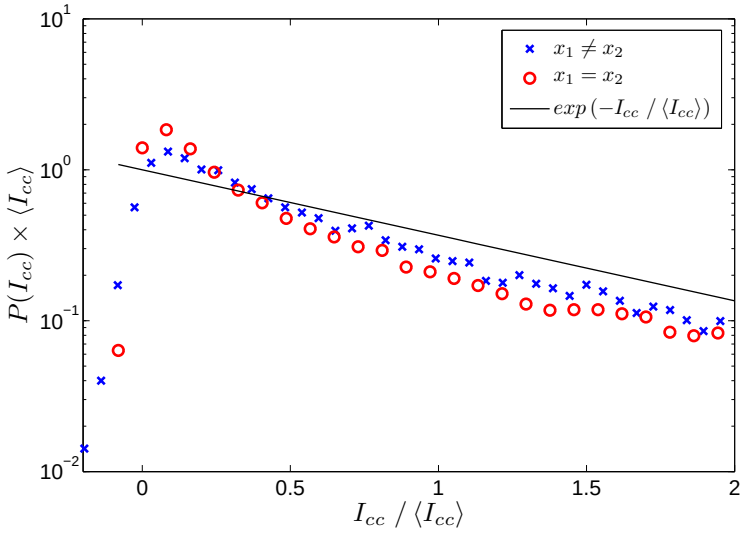

Figure 13: Identical to figure 12, but now plotted on a log scale.

$$\mathcal{V}_{cc}(x_1 \neq x_2) = 1 + \frac{2}{K} \tag{4}$$

$$\mathcal{V}_{cc}(x_1 = x_2) = 1 + \frac{4}{K} \tag{5}$$

We can use these results to calculate the visibilities of our measurements depicted in figures 12 and 13. Of course we can also calculate them directly from our experimental results, using the standard expression of the visibility

$$\mathcal{V} = \frac{\langle I^2 \rangle}{\langle I \rangle^2} - 1 \tag{6}$$

When we put these results next to each other, we obtain table 1. Though we still need to figure out the proper way to calculate error margins for these results, theory and experiment seem to be in reasonable good agreement.

Parameter	Theory	Experiment
$\mathcal{V}_1$	0.67	0.70
$\mathcal{V}_{cc}(x_1 \neq x_2)$	2.3	2.4
$\mathcal{V}_{cc}(x_1 = x_2)$	3.7	4.0

Table 1: Experimental and theoretical results for the visibilities of the single and coincidence statistics ($K = 1.5$ is used for all three theoretical values).

The purity of the state can be be calculated using these results, using

$$P = V_{cc} - 2V_1 \tag{7}$$

Using the experimental results for the case $x_1 \neq x_2$ we find it to be 1, which indicates our state is pure.

We can also use equations 3, 4 and 5 to calculate the experimental number of modes K from the visibilities. The values we find find this way lie between 1.3 and 1.4.

3.4 Discussion

A couple of points warrant further investigation. Firstmost we noticed that our measurements include a small number of points with exceptionally high coincidence counts, and that these high values have a significant influence on our calculated visibilities. When for instance we remove the ten highest count rate values from our data (containing a total of 13699 datapoints), the visibilities for the coincidence measurements become rougly ten percent lower. The single detector visibilities change too, but only a little; about 3 percent. These outlying points we find when both detectors hit a rare but ordinarily high value. We don't know yet how to deal with these points; they might be perfectly natural, but because of their rare occurrence they form an unreliable factor in our statistical analysis. We did not remove them from the analysis.

A second possibility for trouble comes in the form of the calculation of accidental counts. To calculate R_{cc} we take the absolute (uncorrected) coincidence counts reported by the coincidence circuitry, and subtract the accidental counts $R_{acc} = R_1 R_2 \tau_{window}$. We find that a small change in detector gate time τ_{window} has a significant effect on our statistics. A ten percent change of τ_{window} results in a 30 percent change of V_{cc}.

Conclusions

- We have successfully performed a classical enhanced backscattering experiment. We conclude that a two-photon version of the experiment should be experimentally possible, though it might be necessary to simulate a backscattering medium to get a setup with acceptable efficiency.

- A two-photon field can be made to exhibit fermionic or anyonic behaviour by sending it through a dual retarder plate. Normally entangled photons, when sent through a scattering medium, will bunch together on the other end. In the case of fermionic behaviour the photons anti-bunch and in the case of anyonic behaviour, we don't observe any structure at all.

- When working with a very low amount of entangled spatial modes, two-dimensional coincidence speckle patterns can be written as the factorization of two one-dimensional single detector speckle patterns. These speckle patterns clearly exhibit non-exponential statistics. We have measured the single and coincidence visibilities for two cases; one where both detectors look at the same spot and one where they look at different spots. A new theory written to accommodate our measurements seems to be in reasonable agreement with the experimental data.

References

[1] R. Corey, M. Kissner and P. Saulnier, "Coherent bacscattering of light", Am. J. Phys. **63**, 6 (1995)

[2] O. L. Muskens and A. Langendijk, "Broadband enhanced backscattering spectroscopy of strongly scattering media", OSA **16**, 2 (2008)

[3] P. E. Wolf, G. Maret, E. Akkermans and R. Maynard, "Optical coherent backscattering by random media: an experimental study", J. Phys. Fr. **49**, 63 (1988)

[4] E. Jakeman, "Enhanced Backscattering through a deep random phase screen", J. Opt. Soc. Am. A **5**, 10 (1988)

[5] W. H. Peeters, "Two-photon interference, Spatial aspects of two-photon entanglement, diffraction, and scattering", PhD thesis Leiden (2010)

[6] C. W. J. Beenakker, J. W. F. Venderbos and M. P. van Exter, "Two-Photon Speckle as a Probe of Multi-Dimensional Entanglement", Phys. Rev. Letter. **102**, 19 (2010)

[7] C. K. Law and J. H. Eberly, "Analysis and Interpretation of High Transverse Entanglement in Optical Parametric Down Conversion", Phys. Rev. Lett. **92**, 12 (2004)

A Bosonic, fermionic, and anyonic behavior in two-photon scattering

The results of chapter 2 are the subject of a paper. The latest version of this paper, that has as of writing not yet been published, is included for your convenience.

Bosonic, fermionic, and anyonic symmetry in two-photon scattering

M. P. van Exter, J. Woudenberg, H. Di Lorenzo Pires, and W.H. Peeters
(Dated: March 21, 2011)

Bunching and anti-bunching of particles is associated with their bosonic or fermionic nature. This multi-particle behavior is a natural consequence of the symmetry of the total wavefunction under particle exchange. Here, we experimentally study bunching and anti-bunching in a quantum system in which the exchange symmetry can be controlled manually. We use two distinguishable photons and associate their spatial degrees of freedom with the two-particle wavefunction under study. To let the multi-particle behavior reveal itself, we send the two-photon state through a multiple scattering system that randomly mixes the positions of the photons. The scattered photons are observed to cluster together or to avoid each other depending on the imposed symmetry. We also emulate anyonic behavior.

PACS numbers:

Bunching and anti-bunching refer to the increased or decreased probability for two particles to occupy the same quantum state instead of different quantum states. For light, photon bunching was first observed by Hanbury Brown and Twiss [1], in an experiment where they divided light from mercury lamp in two parts and correlated their photon detection events. They later demonstrated the same bunching effect with star light and showed how its spatial dependence can be used to determine the star diameter even in the presence of atmospheric turbulence [2]. Two decades later, photon anti-bunching was demonstrated in the emission of individual atoms, which act as single-photon sources that emit only "one photon at a time" [3].

Photon bunching and anti-bunching effects have also been observed with sources that emit photons only in quantum-entangled pairs. Such photon pair sources generally operate on the nonlinear optical process of spontaneous parametric down-conversion (SPDC), where a single pump photon occasionally splits up in two photons, each carrying approximately half the energy [4]. Hong, Ou, and Mandel [5] demonstrated photon bunching, by combining two photons out of a pair on a beam splitter to show that they always leave via the same output channel and never choose different channels. Later experiments have also demonstrated the occurrence of anti-bunching in two-photon interference when a spatially anti-symmetric pump profile is used [6].

Coherent scattering in random media has attracted lots of interest on account of its intriguing physics, which includes speckle formation [7], conductance fluctuations [8, 9], enhanced backscattering [10], and Anderson localization [11]. Other experiments have focused on multi-particle effects such as the propagation of quantum noise and quantum entanglement through random media [13–16].

This paper describes the statistics of quantum-entangled photon pairs scattered from a random medium. A central concept in the description is the two-photon function $A(\boldsymbol{\rho}_1, \boldsymbol{\rho}_2)$, which is the probability amplitude to observe photon 1 at transverse position $\boldsymbol{\rho}_1$ and photon 2 at $\boldsymbol{\rho}_2$. We find that the natural bosonic symmetry of the input two-photon field ($A(\boldsymbol{\rho}_1, \boldsymbol{\rho}_2) = A(\boldsymbol{\rho}_2, \boldsymbol{\rho}_1)$) survives the ensemble averaging that we apply by rotating the scattering medium. We introduce an experimental technique that allows us to tune the particle symmetry from bosonic to fermionic and anyonic. For an anti-symmetric input field, we observe photon anti-bunching where the photons try to avoid each other and never scatter into identical spatial modes. For anyonic symmetry, we observe how the exchange interaction between the two photons combines effective attraction with repulsion.

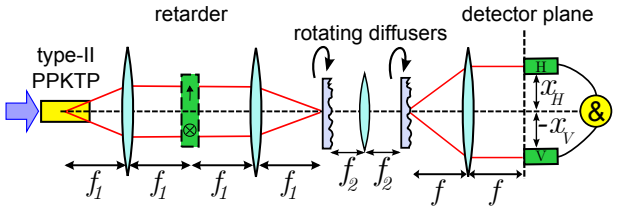

FIG. 1: **Experimental setup**. From left to right: quantum-entangled photon pairs pass through an optional retarder (to modify their state), scatter from a random medium comprising two rotating diffusors, and are detected by two photon counters and coincidence logic.

Figure 1 shows the experimental setup. Pairs of photons, with orthogonal H and V polarization, are generated via SPDC in a nonlinear optical crystal and focused into a scattering medium. The spatial correlation of the scattered photons are measured with two single-photon detectors, located in the far field of the scattering medium and connected to fast electronics that records both individual and coincidence counts. The symmetry of the input two-photon field can be modified by an optional "dual retarder" plate, to be discussed below. We mimic a volume scatterer by two random phase plates positioned in conjugate planes [14]. The limited (1°) scattering angle of these plates strongly enhances the signal. Both plates are rotated to allow ensemble averaging.

The left image in Fig. 2 shows the experimental result obtained without retarder. This false-color plot depicts the coincidence rate $\overline{R_{\rm cc}(x_H, x_V)} \propto \overline{|A(x_H, x_V)|^2}$ as a function of the transverse positions x_H and x_V of the

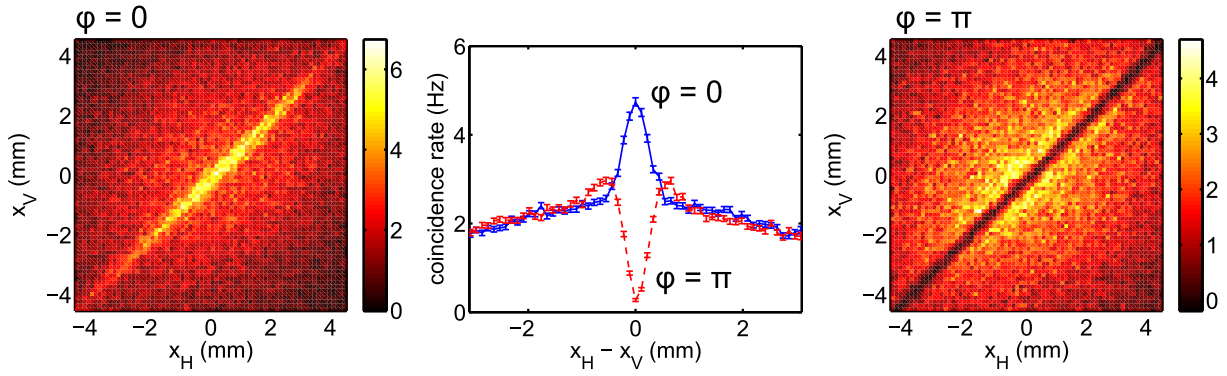

FIG. 2: **Observation of bosonic and fermionic symmerty in two-photon scattering.**(left,right) False-color plots of the coincidence count rate, observed in the far field of a random scattering medium, versus the detector positions x_H and x_V. The (left/right) figure is measured for a (symmetric $\varphi = 0$/anti-symmetric $\varphi = \pi$) two-photon input field. (middle) Projected coincidence rate versus the position difference $x_H - x_V$. The upper (blue) $\varphi = 0$ curve exhibits photon bunching; the lower (red) $\varphi = \pi$ curve exhibits photon anti-bunching.

H- and V-polarized photon in the detector plane, where the bar denotes ensemble averaging. Previous correlation measurements on a stationary scattering medium exhibited two-photon speckle in the absence of one-photon speckle [12, 14]. Being interested in ensemble-averaged pair correlations only, we now apply a sample rotation to average over many ($\gg 100$) speckle patterns. This removes most features from the two-photon speckle, apart from a prominent enhancement along the diagonal $x_H = x_V$.

The enhanced coincidence rate observed along the $x_H = x_V$ diagonal is the photon bunching that we wish to study. For a quantitative analysis, we select data within a rectangular box oriented at 45° and project/average the data along this direction. The upper (blue) curve in the central image of Fig. 2 shows the projected coincidence rate as a function of the position difference $x_H - x_V$. Photon bunching is observed as an increase of the coincidence rate around $x_H - x_V \approx 0$ by a bunching factor $F \equiv \overline{R_{\rm cc}(x_H = x_V)}/\overline{R_{\rm cc}(x_H \neq x_V)} = 1.90 \pm 0.03$ with respect to neighboring values; this is close to the expected value of 2. The width of the bunching peak (FWHM $= 0.54 \pm 0.02$ mm for a high-quality Gaussian fit) denotes the size of a spatial mode. It is comparable to the size of the two-photon speckles observed for a static (non-rotating) sample and Fourier related to the average two-photon illumination on the final diffusor (see supplementary material).

Next, we discuss two-photon scattering of input states with a different symmetry. We modify this symmetry by passing the photon pairs through a custom-made dual retarder plate, comprising two identical zero-order retarders with retardation phase $\varphi/2$ that are rotated 90° with respect to each other and mounted side-by-side to fill two half spaces ($x' < 0$ and $x' > 0$). As the plate is positioned in the far-field of the source and as the emission angles of the photons are anti-correlated, the two photons will generally pass through opposite plate segments. The retardation phases imposed by the dual retarder thereby modify the bosonic symmetry of incident field into a new symmetry

$$A_{\rm plate}(\boldsymbol{\rho}_2', \boldsymbol{\rho}_1') = e^{i\varphi} A_{\rm plate}(\boldsymbol{\rho}_1', \boldsymbol{\rho}_2') \qquad (1)$$

for $x_1' > 0$ and $x_2' < 0$. We will neglect the weak field associated with photon pairs that don't split up, but instead both pass through the same plate segment; the probability of these rare pairs is ≈ 0.05 in our experiment.

After modification, we send the two-photon state through a multiple scattering system that randomly mixes the positions of the photons. Despite this mixing, the symmetry between the two dominant contributions remains intact throughout the system if (as in our case) the propagation and scattering are practically polarization insensitive. The combined two-photon field in any transverse plane that follows can thus be written as

$$A(\boldsymbol{\rho}_1, \boldsymbol{\rho}_2) \approx A_q(\boldsymbol{\rho}_1, \boldsymbol{\rho}_2) + e^{i\varphi} A_q(\boldsymbol{\rho}_2, \boldsymbol{\rho}_1)\,, \qquad (2)$$

where $A_q(\boldsymbol{\rho}_1, \boldsymbol{\rho}_2)$ singles out the scattered field that originates from all photon pairs at positions $x_1' > 0$ and $x_2' < 0$ on the retarder plate.

Figure 3 shows how the observed bunching effects originate from the interference of the field A_q with its mirror image. When the detectors are displaced with respect to each other ($\boldsymbol{\rho}_1 \neq \boldsymbol{\rho}_2$) these two contributions will generally differ and thus sum *incoherently* to the ensemble-averaged signal. At $\boldsymbol{\rho}_1 \approx \boldsymbol{\rho}_2$, however, the field propagators become identical and the ensemble-averaged signal will be the *coherent* sum of the probability amplitudes associated with the two pictures. The two-photon coincidence rate at $\boldsymbol{\rho}_1 \approx \boldsymbol{\rho}_2$ will thus be enhanced by a factor $|1 + \exp(i\varphi)|^2/2 = 1 + \cos\varphi$ as compared to neighboring positions $\boldsymbol{\rho}_1 \neq \boldsymbol{\rho}_2$. Photon bunching occurs for the symmetric ($\varphi = 0$) two-photon input, while anti-bunching occurs for the anti-symmetric ($\varphi = \pi$) input.

The right image in Fig. 2 is a false-color plot of the coincidence rate $R_{\rm cc}(x_H, x_V)$ observed for an anti-symmetric input field ($\varphi = \pi$). A drastic reduction of the

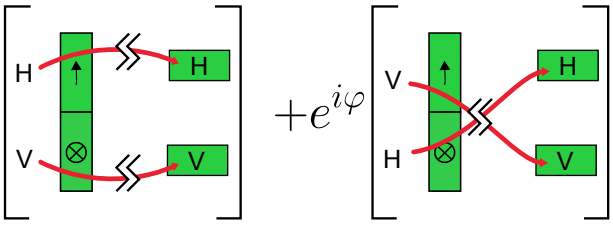

FIG. 3: **Graphical explanation of bunching effect.** The observed bunching effects originate from the interference of two generic scattering paths of the photon pair from the retarder plane (left), via propagation and scattering (denoted by sharp ss-symbols), to the detectors (right).

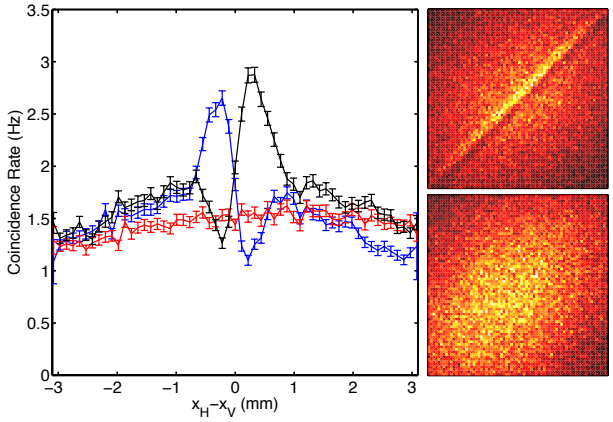

FIG. 4: **Observation of anyonic symmetry in two-photon scattering.** Projected coincidence rate versus the position difference $x_H - x_V$ for an input field with anyonic symmetry. The two wiggly (blue and black) curves are measured for $\varphi = \pi/2$ (original data top right) and $\varphi = -\pi/2$, respectively. The non-wiggly (red) curve is measured while scanning in the orthogonal transverse direction $y_H - y_V$ (original data bottom right).

coincidence count rate is observed for all pairs around the diagonal $x_H = x_V$, irrespective of the individual values of x_H and x_V. We again select a rectangular box, project onto the diagonal, and plot the projected coincidence rate versus the position difference $x_H - x_V$. The lower (red) curve in the central image of Fig. 2 shows the occurrence of photon anti-bunching around $x_H \approx x_V$. The central minimum decreases to a bunching factor $F = 0.09 \pm 0.04$ of neighboring values, to be compared with an ideal value of 0. At a FWHM of 0.40 ± 0.02 μm, the central minimum is slightly narrower than the maximum observed under photon bunching and two small shoulders appear (see supplementary material for discussion).

As a final experiment, we replace our $\varphi = \pi$ plate by a similar $\varphi = \pi/2$ dual retarder plate. This plate transforms the generated state into a two-photon field with the unusual symmetry $A(x_2' < 0, x_1' > 0) = \exp(i\varphi) A(x_1' > 0, x_2' < 0)$, where $\exp(i\varphi) = i$ for the considered $\varphi = \pi/2$. The symmetry of this state interpolates between bosonic and fermionic and can hence be called anyonic.

The term anyon was introduced by Wilczek [17] to describe the statistics of composite quasi-particles in a two-dimensional system, formed by charged particles and flux tubes. These composites behave as quasi-particles with fractional quantum statistic [18, 19], as they acquire a phase factor $\pm\exp(i\varphi)$ upon exchange, where the sign depends on the sense of rotation around the vortex. In solid-state physics, the introduction of anyons is a convenient means to incorporate long-range interactions, associated with the Aharonov-Bohm phase, into the description.[17] Anyonic symmetry in quantum optics was previously introduced as a means to describe interference in four- and six-photon events [20, 21]. Our experiment shows that anyonic symmetry is also relevant for the scattering statistics of entangled photon pairs.

Figure 4 shows the results obtained under illumination with a two-photon field with anyonic symmetry ($\varphi = \pi/2$). The inset is a false-color plot of the coincidence count rate versus the detector positions. The main figure shows a diagonal projection of this data, using the method described earlier. The two wiggly (blue and black) curves are obtained for two different orientation of the retarder plate, where the front side of the plate was facing either the source or the scattering medium. These two curves are approximate mirror images, in agreement with the inversion ($\varphi \to -\varphi$) or ($x \to -x$) associated with the reorientation of the plate. Each curve demonstrates an intriguing combination of bunching and anti-bunching. The exchange interaction between the two photons is now asymmetric, such that the H-polarized photon prefers to be on the righthand side of the V-polarized photon, but avoids the lefthand side for one orientation of the plate, and vice versa for the other orientation. This unusual asymmetry originates from the spatial structure of the A_q-field at the second diffusor (see supplementary material); it disappears at increased scattering angles and is absent if we scan the detectors in the orthogonal transverse direction $y_H - y_V$ (see red non-wiggly curve in Fig. 4).

From a general perspective, our experiments demonstrate the importance of exchange symmetry in multi-particle scattering. For the extreme cases of Bosonic ($\varphi = 0$) and Fermionic ($\varphi = \pi$) symmetry, this exchange symmetry applies to any $(\boldsymbol{\rho}_1, \boldsymbol{\rho}_2)$ combination and Eqs. (1) and (2) are equivalent. For intermediate symmetries ($0 < \varphi < \pi$) only the more general Eq. (2) applies. To quantify the exchange symmetry also for these cases, we introduce the global (spatially-averaged) symmetry parameter

$$S \equiv \frac{\int\int A^*(\boldsymbol{\rho}_2, \boldsymbol{\rho}_1) A(\boldsymbol{\rho}_1, \boldsymbol{\rho}_2) d\boldsymbol{\rho}_1 d\boldsymbol{\rho}_2}{\int\int |A(\boldsymbol{\rho}_1, \boldsymbol{\rho}_2)|^2 d\boldsymbol{\rho}_1 d\boldsymbol{\rho}_2}. \qquad (3)$$

This real-valued symmetry parameter S is conserved under unitary scattering and propagation if these processes are identical for both particles. The parameter S determines the bunching factor after random scattering via $F \approx 1 + S$. For our system $S = \cos\varphi$, with fermionic ($S = -1$) and bosonic ($S = 1$) symmetry as extreme

cases.

In conclusion, bunching effects are inevitable in multi-particle scattering. In our description of the field of two distinguishable (H and V polarized) photons these bunching effects originate from the conservation of the global symmetry S and its link to particle exchange.

We acknowledge support from the Stichting voor Fundamenteel Onderzoek der Materie (FOM) and the EU under the FET-Open Agreement HIDEAS, No. FP7-ICT-221906.

I. METHODS

Photon pairs are generated in a 5-mm long periodically-poled KTP crystal, using a 200 mW cw single-mode beam from a Krypton ion laser operating at a wavelength of 413 nm. The crystal is phase matched for frequency-degenerate type-II spontaneous parametric down-conversion, generating pairs of photons of opposite (H, V) polarization at $\lambda \approx 826$ nm. The pump light is remove with an AR-coated GaP wafer positioned behind the KTP crystal, while the frequency-degenerate photon pairs are selected with narrow-band ($\Delta\lambda = 1$ nm) interference filters. A polarizing beam splitter (not shown in Fig. 1) separates the scattered H and V photons before detection and allows us to position the two single-photon detectors effectively on top of each other. Each detector is connected to a single-mode optical fiber, whose compact image can be scanned in the far-field plane of the scattering medium. The detector modes are small enough (140 μm) to allow for accurate imaging in the detector plane, but large enough to collect enough light. All discussed two-photon features are observed in the absence of one-photon speckle, at approximately constant single-photon count rate, and after subtraction of a small fraction (≈ 10 %) of accidental coincidence counts. Integration times are typically 12 s per date point.

II. SUPPLEMENTARY MATERIAL

The observed bunching effects originate from the interference between the two dominant contributions to the speckle field given in Eq. (2). The symmetry between these contributions allows us to express the spatial structure of the bunching effect in terms of the ensemble-averaged correlation between the speckle fields $A_q(\boldsymbol{\rho}_1, \boldsymbol{\rho}_2)$ and its mirror image $\exp(i\varphi)A_q(\boldsymbol{\rho}_2, \boldsymbol{\rho}_1)$, such that

$$\overline{R_{\rm cc}(\boldsymbol{\rho}_1, \boldsymbol{\rho}_2)} \propto \left(1 + {\rm Re}[e^{i\varphi}\mu(\boldsymbol{\rho}_1 - \boldsymbol{\rho}_2, \boldsymbol{\rho}_2 - \boldsymbol{\rho}_1)]\right) , \quad (4)$$

where the normalized correlation function $\mu(\boldsymbol{\rho}_1 - \boldsymbol{\rho}_2, \boldsymbol{\rho}_2 - \boldsymbol{\rho}_1) \propto \langle \overline{A_q^*(\boldsymbol{\rho}_1, \boldsymbol{\rho}_2) A_q(\boldsymbol{\rho}_2, \boldsymbol{\rho}_1)} \rangle$. This correlation function is Fourier related to the illumination profile at the final diffusor [14], or more precise to that part of the illumination rate $R_{\rm cc}$ that originates only from $A_q(\boldsymbol{\rho}_1, \boldsymbol{\rho}_2)$. Hence we expect approximately equal widths and shapes for the bunching structures observed for bosonic and fermionic states. Both measured widths (0.54 ± 0.02 μm and 0.40 ± 0.02 μm) are indeed comparable to the typical speckle size observed for a static medium and as expected from the above Van Cittert-Zernike type argument [14]. We attribute the somewhat smaller width of the fermionic structure and its additional weak shoulder (a remnant of photon bunching) to the small contribution of photon pairs with $x_1'.x_2' > 0$ that we neglected in the main text. Both aspects also show up in numerical calculations that simulate our system in one transverse dimension.

The intriguing wiggle in the anyonic curve also follows naturally from Eq. (4). It originates from an asymmetry in the (A_q-part of the) illumination profile $R_{\rm cc}$ at the final diffusor, which translates into a complex and asymmetric correlation function $\mu(\boldsymbol{\rho}_1 - \boldsymbol{\rho}_2, \boldsymbol{\rho}_2 - \boldsymbol{\rho}_1)$ for $x_1 \neq x_2$. Our simulations show that this asymmetry is a remnant of the spatial separation imposed by the dual retarder plate that is still visible at the second diffusor on account of the limited (1°) scattering angle of the first diffusor plate. The wiggle disappears if we increase the scattering angle of the plates in the computer or if we scan in the y instead of the x direction. It also disappears if we add a third scattering plate to the simulations. In contrast, the bosonic and fermionic bunching features survive both modifications of the scattering. These observations show that the bosonic and fermionic symmetries are in a way more fundamental than the anyonic symmetry. The first two are global exchange symmetries, where Eq. (1) is valid in any transverse plane. The anyonic symmetry, on the other hand, is local in the sense that Eq. (1) is valid only in the retarder plane, where the available phase space separates in two natural segments, but has to be replaced by the more general Eq. (2) for consecutive planes. After sufficient scattering, the exchange contributions with phase factors $\exp(i\varphi)$ and $\exp(-i\varphi)$ combine to the global symmetry parameter $S = \cos\varphi$, as conserved quantity, and an associated bunching factor $F \approx 1 + S$.

[1] Hanbury Brown, R. & Twiss, R.Q., Correlation between photons in two coherent beams of light. *Nature* **177**, 27-29 (1956).

[2] Hanbury Brown, R. in *The Intensity Interferometer: its application to astronomy* (Taylor and Francis, London, 1974).

[3] Kimble, H.J., Dagenais, M. & Mandel, L. Photon antibunching in resonance fluorescence. *Phys. Rev. Lett.* **39**, 691-694 (1977).

[4] Kwiat, P.G., Mattle, K., Weinfurter, H., Zeilinger, A., Sergienko, A.V., & Shih, Y.H. New high-intensity source of polarization-entangled photon pairs. *Phys. Rev. Lett.* **75**, 4337-4340 (1995).

[5] Hong, C.K., Ou, Z.Y. & Mandel, L. Measurement of subpicosecond time intervals between two photons by interference. *Phys. Rev. Lett.* **59**, 2044-2047 (1987)

[6] Nogueira, W.A.T., Walborn, S.P., Pádua, S. & Monken, C.H. Generation of two-photon singlet beam. *Phys. Rev. Lett.* **92**, 043602 (2004).

[7] Goodman, J.W. Some fundamental properties of speckle. *J. Opt. Soc. Am.* **66**, 1145-1150 (1976).

[8] Washburn, S. & Webb, R.A. Quantum transport in small disordered samples from the diffusive to the ballistic regime, *Rep. Prog. Phys.* **55**, 1311-1383 (1992).

[9] Beenakker, C.W.J. Random-matrix theory of quantum transport. *Rev. Mod. Phys.* **69**, 731-808 (1997).

[10] Van Albada, M.P. & Lagendijk A. Observation of Weak Localization of Light in a Random Medium. *Phys. Rev. Lett.* **55**, 26922695 (1985).

[11] Wiersma, D.S., Bartolini, P., Lagendijk, A. & Righini, R. Localization of light in a disordered medium, *Nature* **390**, 671-673 (1997).

[12] Beenakker, C.W.J., Venderbos, J.W.F. & van Exter, M.P. Two-Photon Speckle as a Probe of Multi-Dimensional Entanglement. *Phys. Rev. Lett.* **102**, 193601 (2009).

[13] Lodahl, P. & Lagendijk, A. Transport of quantum noise through random media. *Phys. Rev. Lett* **94**, 153905 (2005).

[14] Peeters, W.H., Moerman, J.J.D. & van Exter, M.P. Observation of Two-Photon Speckle Patterns, *Phys. Rev. Lett.* **104**, 173601 (2010).

[15] Ott, J.R., Mortensen, N.A., & Lodahl P. Quantum interference and entanglement induced by multiple scattering of light. *Phys. Rev. Lett* **105**, 090501 (2010).

[16] Lahini, Y., Bromberg, Y., Christodoulides, D. N., & Silberberg, Y. Quantum Correlations in Two-Particle Anderson Localization, *Phys. Rev. Lett.* **105**, 163905 (2010).

[17] Wilczek, F. Quantum mechanics of fractional spin particles. *Phys. Rev. Lett.* **49**, 957-960 (1982).

[18] Laughlin, R.B. Anomalous quantum Hall effect: an incompressible quantum fluid with fractionally charged excitations. *Phys. Rev. Lett.* **50**, 1395-1398 (1983).

[19] Halperin, B.I. Statistics of quasiparticles and the hierarchy of fractional quantized Hall states. *Phys. Rev. Lett.* **52**, 1583-1586 (1984).

[20] Pachos, J.K. et al. Revealing anyonic features in a toric code quantum simulation, *New J. Phys.* **11**, 083010 (2009).

[21] Lu, C-Y., Gao, W-B., Gühne, O., Chen, Z-B. & Pen, J-W. Demonstrating anyonic fractional statistics with a six-qubit quantum simulator, *Phys. Rev. Lett.* **102**, 030502 (2009).

[22] Jeltes, T. et al. Comparison of the Hanbury Brown-Twiss effect for bosons and fermions, *Nature* **445**, 402 (2007).

[23] Peeters, W.H. Two-photon interference, *PhD thesis, Leiden University* 2010.

B Statistical properties of non-local speckles

The results of chapter 3 are the subject of a paper. The latest version of this paper, that has as of writing not yet been published, is included for your convenience.

Statistical properties of non-local speckles

H. Di Lorenzo Pires, J. Woudenberg, and M. P. van Exter
Leiden University, Huygens Laboratory, P.O. Box 9504, 2300 RA Leiden, The Netherlands
(Dated: April 12, 2011)

We experimentally study the statistics of non-local speckle patterns, obtained when spatially entangled photon pairs are scattered through a random medium. Striking differences arise between the scattering of highly entangled states and almost separable states. Both the purity of the field and the Schmidt number, which quantifies the number of entangled modes, can be obtained from the visibility of the speckles. We observe non-exponential statistics for both the intensities and the two-photon correlations.

PACS numbers: 42.50.Dv, 42.25.Dd, 42.30.Ms, 42.65.Lm

Introduction – Speckles are the random intensity patterns that appear when a wave is reflected from or transmitted through a random scattering medium [1, 2]. At the time of its discovery, speckles were mainly seen as a drawback in coherent imaging systems. Further studies revealed, however, that the speckle pattern carries information both on the coherence properties of the radiation and on the microscopic details of the scattering object. After averaging over many realizations of the disorder, useful information can be retrieved through statistical arguments. The study of wave propagation in random media has revealed many interesting phenomena, such as conductance fluctuations [3, 4], enhanced backscattering [5], and Anderson localization [6].

More recently, considerable effort has been devoted to understand how the quantum nature of light manifests after multiple scattering [7–18]. A broad range of subjects have been investigated, such as the degradation of polarization entanglement [7–9], the transport of quantum noise [10, 11], and the dynamics of photons in disordered lattices [12]. It has also been shown that entanglement can be induced by multiple scattering of squeezed states and that quantum interference can survive ensemble average [16, 17].

The special features of scattering of quantum light are best appreciated in the spatial domain. When a pure two-photon state is scattered by a random medium, it will produce so-called "two-photon speckles" [18]. These patterns are remarkable because they exist in the more abstract space of fourth-order correlations. They show up in the coincidence count rate of two (scanning) detectors and are a function of two position coordinates.

In this Letter we present the first experimental investigation of the statistics of two-photon speckles. We show that either non-local or separable speckle patterns can be observed, depending on the degree of spatial entanglement of the initial state. By averaging over many realizations of the disorder, important properties of the source can be retrieved. In this way, the two-photon state can be proven to be pure and the Schmidt number K, which quantifies the number of entangled modes, can be obtained. Experimentally quantifying multidimensional entanglement is an important, but very demanding task [19]. Our approach provides a feasible and theoretically sound solution for this problem. Finally, we recover the probability distributions of single-photon intensities and two-photon coincidences, which, contrary to most classical speckles, are in general non exponential.

Theory – Statistical distributions of two-photon speckles were first theoretically discussed by Beenakker *et al.* [15]. In this Letter we will greatly benefit from their results. But in order to extend their conclusions to more realistic experimental conditions, our analysis will deviate at several points. First of all, we do not use a random matrix description, with its discrete number of input and output channels, but instead we use a continuous description. The only requirement we will impose on the scattering is that it is sufficiently random and unitary (i.e. energy conserving). Second, we will start from the most general pure input state, whose Schmidt coefficients are not necessarily equal, i.e., we show how the *Schmidt number* K can be measured, instead of the *Schmidt rank*. Finally, we do not separate the two-photon phase space into half-spaces, $q > 0$ and $q < 0$. This allows us to investigate separable states ($K = 1$) as well.

We begin by reviewing some properties of classical speckles. When a field $f(\boldsymbol{x})$ is scattered by a random medium, all possible light paths will acquire arbitrary phases. When these components are added together, they will form a complex interference pattern known as speckle. For unitary scattering, we can describe this pattern by the transformation $F(\boldsymbol{x}) = \mathcal{U}[f(\boldsymbol{x})]$. If the number of scattering centers is very large, the Central Limit Theorem assures that the probability density function for both the real and imaginary components of $F(\boldsymbol{x})$ is asymptotically Gaussian. The intensity $I = |F|^2$ then has an exponential distribution $P(I) \propto \exp(-I/\langle I\rangle)$, with average $\langle I\rangle$. The visibility or contrast of any speckle pattern is defined by $\mathcal{V} = \langle I^2\rangle / \langle I\rangle^2 - 1$, where the brackets denote ensemble average. The exponential distribution has unity visibility.

These results can be generalized to a *two-photon field* $A(\boldsymbol{x}_1, \boldsymbol{x_2})$, which describes the probability amplitude of finding one photon at transverse position $\boldsymbol{x}_1$ and the other at $\boldsymbol{x}_2$. The quantum-entangled nature of the state is best appreciated in the so-called Schmidt decomposition [20], where the two-photon state is expressed as a discrete sum over factorizable two-photon states of the

form $A_k(\boldsymbol{x}_1, \boldsymbol{x}_2) = f_k(\boldsymbol{x}_1) g_k(\boldsymbol{x}_2)$. Part of the beauty of the Schmidt decomposition is that it remains intact upon unitary scattering, as orthogonal states remain orthogonal under this scattering; only the eigenstates are modified. If we write the input state in the Schmidt form, the output state will be

$$A_{out}(\boldsymbol{x}_1, \boldsymbol{x_2}) = \sum_k \lambda_k \, F_k(\boldsymbol{x}_1) G_k(\boldsymbol{x}_2), \tag{1}$$

where λ_k are the Schmidt coefficients and, analogously to the classical case, $F_k(\boldsymbol{x}) = \mathcal{U}[f_k(\boldsymbol{x})]$ and $G_k(\boldsymbol{x}) = \mathcal{U}[g_k(\boldsymbol{x})]$ are the speckle fields corresponding to the transformation of the Schmidt modes f_k and g_k. The coincidence rate measured by two photon counters at positions $\boldsymbol{x}_1$ and $\boldsymbol{x}_2$ is $R_{cc}(\boldsymbol{x}_1, \boldsymbol{x_2}) \propto |A_{out}(\boldsymbol{x}_1, \boldsymbol{x_2})|^2$. If the initial state is separable, i.e., just one term in the Schmidt decomposition, the two-photon speckles observed in R_{cc} will also be separable. On the other hand, if the input state is highly entangled, R_{cc} will reveal a *nonlocal* speckle pattern. The effective number of entangled modes in the decomposition (1) is usually quantified by the Schmidt number $K = 1/\sum_k |\lambda_k|^4$. The Schmidt coefficients are normalized such that $\sum_k |\lambda_k|^2 = 1$.

We will now study the statistics of the intensities I (single photon rate) and of the coincidences R_{cc}. From Eq. (1) we immediately obtain

$$R_{cc} = \alpha \sum_{j,k} \lambda_j^* \lambda_k \, F_j^* F_k G_j^* G_k, \tag{2}$$

$$R_{cc}^2 = \alpha^2 \sum_{i,j,k,m} \lambda_i^* \lambda_j^* \lambda_k \lambda_m \, F_i^* F_j^* F_k F_m G_i^* G_j^* G_k G_m, \tag{3}$$

where we omit the coordinates $\boldsymbol{x}_1$ and $\boldsymbol{x}_2$. The proportionality constant α incorporates the experimental factors that relate the theory to the measured coincidences rate. Let's first assume that $\boldsymbol{x}_1 \neq \boldsymbol{x}_2$. In this case, the speckle fields F and G are statistically independent. Furthermore, the fields F_i and F_j are also statistically independent, unless $i = j$. The same holds for G. Due to the Gaussian-random nature of the scattered fields, $\langle |F_i|^{2n} \rangle = \langle I^n \rangle = n!$, where I is the exponentially distributed intensity, but $\langle F_i^{2n} \rangle = 0$. With these ingredients, it is straightforward to show that

$$\text{For} \quad \boldsymbol{x}_1 \neq \boldsymbol{x}_2 \qquad \begin{cases} \langle R_{cc} \rangle = \alpha, \\ \mathcal{V}_c = 1 + \dfrac{2}{K}, \end{cases} \tag{4}$$

where K is the Schmidt number and $\mathcal{V}_c$ is the visibility of the two-photon speckle pattern. We see that $\mathcal{V}_c$ varies from 3 (separable state) to 1 (maximally entangled state).

The single photon intensities can be obtained by a partial trace of the two-photon state as

$$I_{out}(\boldsymbol{x}) = \sum_k |\lambda_k|^2 \, |F_k(\boldsymbol{x})|^2 = \sum_k |\lambda_k|^2 \, |G_k(\boldsymbol{x})|^2, \tag{5}$$

which is an incoherent sum of many speckle patterns. The more terms in the distribution, the more uniform the intensity becomes. The visibility of the one-photon speckle reduces with the number of modes as

$$\mathcal{V}_I = \frac{1}{K}. \tag{6}$$

When the number of terms in (5) is very large, the Central Limit Theorem can be used to show that $P(I)$ is normally distributed with mean $\langle I \rangle$ and standard deviation $1/\sqrt{K}$.

We have assumed so far that the input state is pure. In a more general sense, the purity $\mathcal{P}$ of the two-photon state can be calculated from the visibilities $\mathcal{V}_I$ and $\mathcal{V}_c$ of the single-photon and two-photon speckles as

$$\mathcal{P} = \mathcal{V}_c - 2\mathcal{V}_I. \tag{7}$$

This crucial result, which was first derived in [15], can also be proven using our formalism.

The probability distributions for R_{cc} and I can be deduced from Eqs. (2) and (5), which are weighted sums of products of random Gaussian variables. For the special case of K equally weighted Schmidt modes, with

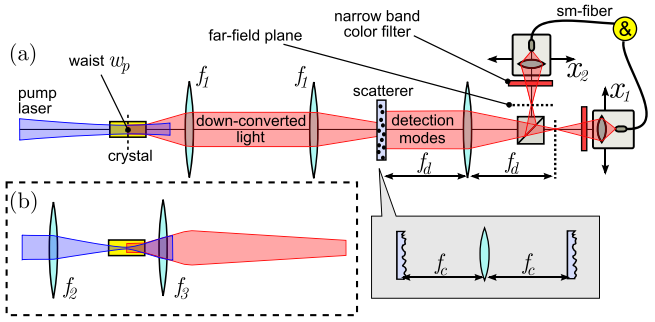

FIG. 1: (Color online) Entangled photon pairs are obtained via type I SPDC by pumping a 5-mm thick periodically poled KTP crystal with a laser beam ($\lambda_p = 413.1$ nm and 200 mW power). The crystal center is imaged onto the incident plane of the scatterer with two $f_1 = 200$ mm lenses. The far field of the scattering medium is imaged with a $f_d = 250$ mm lens onto the detection plane. Detection occurs via projection onto two single-mode fibers. The size of the detection modes ($w_{det} = 140$ μm) determines the spatial resolution in the far-field plane. Narrow band spectral filters (5 nm at 826.2 nm) are used to selected down-converted light close to frequency degeneracy. The inset shows our scattering medium, which comprises two light shaping diffusers positioned in each other's far field (using a lens $f_c = 10$ mm). This configuration mimics a volume scatter [18], but it also allows sufficient counts to be measured. (a) Generation of a state with $K_{th} = 80$. The pump is weakly focused to a waist $w_p = 160$ μm. (b) Generation of a state with $K_{th} = 1.4$. The pump lens (not shown) is removed and a $f_2 = 100$ mm lens focuses the beam to a spot $w_p = 11.5$ μm at the center of the crystal. The two f_1 lenses are removed and a single $f_3 = 59$ mm lens images the center of the crystal on the scatter.

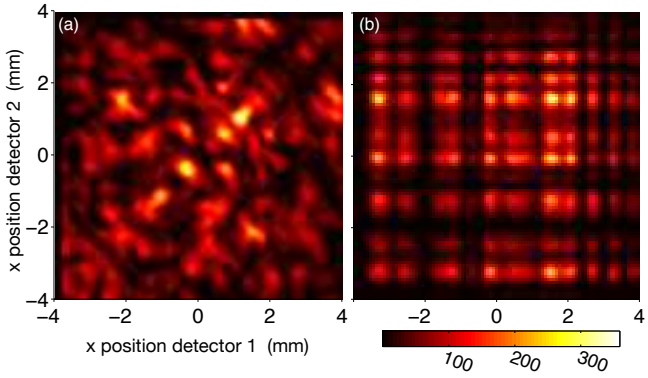

FIG. 2: (Color online) Coincidence counts measured by two scanning detectors for a single realization of the scattering medium. (a) A non-local speckle pattern, corresponding to the scattering of a highly entangled state with $K_{th} = 80$. (b) Separable speckle pattern, corresponding to the scattering of a state with a small number of modes, $K_{th} = 1.4$.

$\lambda_k = 1/\sqrt{K}$, we recover the closed expressions of Ref. [15]

$$P_1(\tilde{I}) = \tilde{I}^{K-1}\frac{e^{-K\tilde{I}}K^K}{\Gamma(K)}, \quad (8)$$

$$P_2(\tilde{R}_{cc}) = \frac{K}{\Gamma(K)}(K\tilde{R}_{cc})^{\frac{K-1}{2}}\mathcal{K}_{K-1}\left[2\sqrt{K\tilde{R}_{cc}}\right], \quad (9)$$

where $\tilde{I} = I/\langle I\rangle$ and $\tilde{R}_{cc} = R_{cc}/\langle R_{cc}\rangle$, Γ is the Gamma function and $\mathcal{K}_{K-1}$ is a modified Bessel function of the second kind. The single-photon probability density $P_1(\tilde{I})$ is a Gamma distribution while, the two-photon probability $P_2(\tilde{R}_{cc})$ is known as the "K"-distribution [21].

We finally consider the case $\boldsymbol{x}_1 = \boldsymbol{x}_2 = \boldsymbol{x}$. Because of the symmetry $A(\boldsymbol{x}_1, \boldsymbol{x_2}) = A(\boldsymbol{x}_2, \boldsymbol{x}_1)$ of the two-photon field, the Schmidt modes $F_i(\boldsymbol{x})$ and $G_j(\boldsymbol{x})$ are not all statistically independent. Taking this into consideration, we can repeat the steps above and show that Eqs. (4) and (9) retain their form, but with the substitution $K \to K/2$, which implies that $\mathcal{V}_c = 1+\frac{4}{K}$. The average $\langle R_{cc}\rangle = 2\alpha$ is twice as large. This photon bunching effect survives averaging over many realizations of the disorder.

Experimental results – Figure 1 shows the experimental setup used to generate entangled photon pairs and to measure the statistics of the speckles. We investigate two different regimes, namely, a highly entangled state with theoretical Schmidt number $K_{th} = 80$ and an almost separable state with $K_{th} = 1.4$.

Figure 2 shows measurements of two-photon speckle patterns for a fixed realization of the scattering medium. These figures are obtained by scanning both detectors horizontally, keeping $y_1 = y_2$ fixed, and recording the coincidences count rate. The results are corrected for accidental counts. Figure 2(a) corresponds to a highly entangled state, while Fig. 2(b) shows the results for an almost separable state. The differences are striking. When operating under reduced number of modes, the coincidences rate is practically separable in the product of single-photon intensities, $R_{cc}(x_1, x_2) \approx I(x_1)I(x_2)$. On the other hand, when the number of modes is very large the pattern is clearly non-separable. By measuring photon 1 at a certain position, photon 2 is "nonlocally" projected into a speckle pattern that depends on the position of detector 1. Notice also that both patterns are symmetric with respect to the $x_1 = x_2$ diagonal; this reflects the symmetry of the field $A(\boldsymbol{x}_1, \boldsymbol{x_2}) = A(\boldsymbol{x}_2, \boldsymbol{x}_1)$.

TABLE I: Overview of the measured statistics, obtained for $x_1 \neq x_2$. The theoretical Schmidt number K_{th} is calculated via the procedure in [20]; $\mathcal{V}_I$ and $\mathcal{V}_c$ are the visibilities of the intensities and coincidences respectively, $\mathcal{P}$ is the purity, and K_{ex} is the measured Schmidt number.

K_{th}	$\mathcal{V}_I$	$\mathcal{V}_c$	$\mathcal{P}$	K_{ex}
1.4	0.83 ± 0.02	2.65 ± 0.15	0.98 ± 0.15	1.20 ± 0.03
80	0.014 ± 0.002	1.04 ± 0.04	1.01 ± 0.04	70 ± 9

We will next discuss the statistical distributions of the coincidences R_{cc} and intensities I under various conditions. To this end, the detectors are placed at fixed positions, either $x_1 = x_2$ or $x_1 \neq x_2$. Different realizations of disorder are obtained by rotating the first or the second diffuser in steps of 3°. In this way, we can measure 14,400 realizations of the scattering medium. The acquisition time for each measurement was 5 seconds. An overview of the results for $x_1 \neq x_2$ is shown in table I.

Figure 3 shows the probability distributions measured for $K_{th} = 1.4$, i.e., for an almost separable state. The dashed red curves are the theoretical curves, obtained using Eqs. (8) and (9) with the measured Schmidt number K instead. The dashed black lines correspond to an exponential distribution and confirm that all three distributions are non-exponential. When $K_{th} = 1.4$, the field is not only coherent in fourth order, but it is also almost coherent in second order. The single photon speckles exhibit high visibility, $\mathcal{V}_I = 0.83 \pm 0.02$, not very far from unity visibility, which holds for completely coherent light. This visibility allows us to estimate the experimental Schmidt number to be $K = 1.20 \pm 0.03$, confirming that our state is practically separable. The associated probability distribution P_1 is shown in Fig. 3(a). The distribution is slightly concave on a semi-log scale and is theoretically described by a Gamma distribution. This distribution would have been exactly exponential in the limit $K = 1$.

The results for the coincidence counts are more interesting. Figure 3(b) shows the probability distribution P_2 of two-photon speckles for $x_1 \neq x_2$. The associated visibility $\mathcal{V}_c = 2.65 \pm 0.15$ has a relatively large error margin. The main reason for this error is the occurrence of a few very large fluctuations, associated with the extreme tail of the P_2 distribution. As we can see, the distribution has a convex shape on a semi-log scale, such that the probability of very small *and* very high fluctuations are higher than for an exponential distribution. The error in

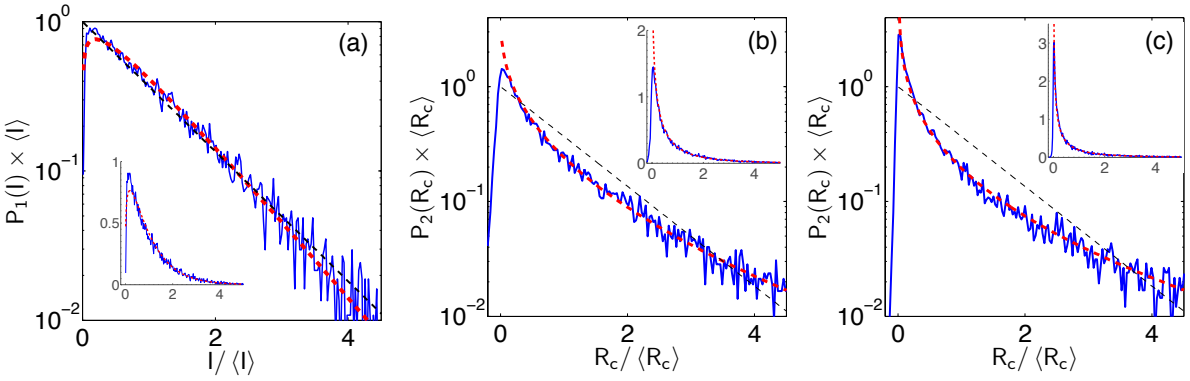

FIG. 3: (Color online) Probability distributions measured for $K_{th} = 1.4$. The (red) dashed curves are the theoretical distributions and the (black) dashed lines correspond to an exponential distribution. The insets show the results on a linear scale. (a) Distribution P_1 of intensities. (b) Distribution P_2 of coincidences for $x_1 \neq x_2$. (c) Distribution P_2 of coincidences for $x_1 = x_2$.

$\mathcal{V}_c$ will propagate to the purity $\mathcal{P}$. We obtain an average value $\mathcal{P} = 0.98 \pm 0.15$ for the purity of the two-photon state.

Figure 3(c) shows the probability distribution of R_{cc} for $x_1 = x_2$. The convexity is even more pronounced and the peak close to $R_{cc} \approx 0$ is twice as large, as can be seen in the insets. Theoretically, the peak at $R_{cc} = 0$ should be much higher. The measured shape and peak around $R_{cc} = 0$, however, are limited by the experimental noise that inevitably dominates at the smallest count rates. The two-photon speckle contrast is $\mathcal{V}_c = 4.45 \pm 0.30$, which reflects the almost classical, i.e local, nature of the fluctuations. For a fully factorizable speckle, the visibility of $R_{cc} \approx I^2$ is $\mathcal{V}_| = 5$.

Figure 4 shows the probability distributions for a highly entangled state with $K_{th} = 80$. In the limit of high K, the two-photon speckles are a genuine two-coordinate function and can be considered as a more authentic generalization of classical speckles to fourth-order optics. The fluctuations at $x_1 = x_2$ are now not more special than those at $x_1 \neq x_2$; only the average level will be different due to the photon bunching effect. The probability distribution P_2 for $x_1 \neq x_2$, shown in Fig. 4(a), is practically exponential and the visibility $\mathcal{V}_c = 1.04 \pm 0.04$ is close to unity. Extreme fluctuations do not occur very often for this distribution. As a result, the error in $\mathcal{V}_c$ is smaller. The distributions for $x_1 = x_2$ and $x_1 \neq x_2$ have approximately the same shape, but since the number of modes is still finite, the visibility for $x_1 = x_2$ is slightly higher, namely, $\mathcal{V}_c = 1.10 \pm 0.05$.

Figure 4(b) shows the probability distribution P_1 on a linear scale. Because the reduced one-photon state is now practically incoherent, the intensity will exhibit only limited fluctuations around the average $\langle I \rangle$. As expected from the Central Limit Theorem, the curve is approximately Gaussian. The associated one-photon visibility is only $\mathcal{V}_I = 0.014 \pm 0.002$. To measure this value, we had to correct for a small wedge effect in the diffusors. This correction introduces a relative larger error, which propagates when calculating the Schmidt number. Nonetheless, the obtained value $K_{ex} = 70 \pm 9$ agrees reasonably well with the large number of modes expected. Finally, we obtain $\mathcal{P} = 1.01 \pm 0.04$ for the purity of the state.

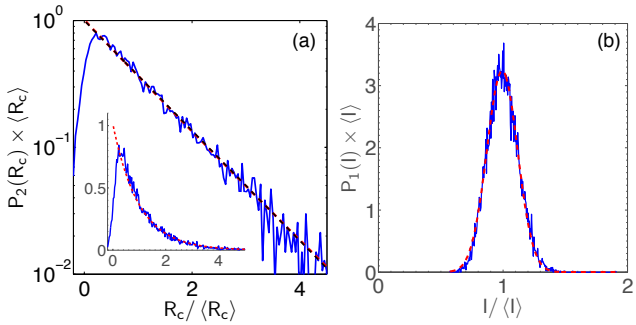

FIG. 4: (Color online) Probability distributions measured for $K_{th} = 80$. The (red) curves are the theoretical distributions and the (black) dashed lines correspond to an exponential distribution. (a) Distribution P_2 of coincidences for $x_1 \neq x_2$. (b) Distribution P_1 of intensities.

Conclusion – We have studied the statistics of two-photon speckle patterns. These patterns are a generalization of classical speckles to fourth-order optics. Depending on the degree of spatial entanglement of the input state, the scattered field can exhibit very different structures and statistics. We have measured the Schmidt number of both an almost separable state and a highly entangled state. We have also proven that both generated states are pure to a good degree of accuracy. These results provide new insights into the role of spatial entanglement to the scattering of light and opens the door to new developments in the field of quantum optics in random media.

The authors acknowledge fruitful discussions with Wouter H. Peeters. This work has been supported by the Stichting voor Fundamenteel Onderzoek der Materie (FOM) and by the EU under the FET-Open Agreement HIDEAS, No. FP7-ICT-221906.

[1] J. W. Goodman, *Speckle Phenomena in Optics: Theory and Applications* (Roberts & Company, Greenwood Village, CO, 2007).
[2] J. W. Goodman, Opt. Soc. Am. **66**, 1145 (1976).
[3] S. Washburn and R. A. Webb, Rep. Prog. Phys. **55**, 1311 (1992).
[4] C. W. J. Beenakker, Rev. Mod. Phys. **69**, 731(1997).
[5] M. P. Van Albada and A. Lagendijk , Phys. Rev. Lett. **55**, 2692 (1985).
[6] D. S. Wiersma *et al.*, Nature **390**, 671 (1997).
[7] A. Aiello and J. P. Woerdman, Phys. Rev. A 70, 023808 (2004).
[8] J. L. van Velsen and C. W. J. Beenakker, Phys. Rev. A **70**, 032325 (2004).
[9] G. Puentes *et al.*, Phys. Rev. A **75**, 032319 (2007).
[10] P. Lodahl and A. Lagendijk, Phys. Rev. Lett. **94**, 153905 (2005).
[11] M. Patra and C. W. J. Beenakker, Phys. Rev. A **61**, 063805 (2000).
[12] Y. Lahini *et al.*, Phys. Rev. Lett. **105**, 163905 (2010).
[13] P. Lodahl, A. P. Mosk, and A. Lagendijk, Phys. Rev. Lett. **95**, 173901 (2005).
[14] S. E. Skipetrov, Phys. Rev. A **75**, 053808 (2007).
[15] C. W. J. Beenakker, J. W. F. Venderbos, and M. P. van Exter, Phys. Rev. Lett. **102**, 193601 (2009).
[16] S. Smolka *et al.*, Phys. Rev. Lett. **102**, 193901 (2009).
[17] J. R. Ott, N. A. Mortensen, and P. Lodahl, Phys. Rev. Lett **105**, 090501 (2010).
[18] W. H. Peeters, J. J. D. Moerman, and M. P. van Exter, Phys. Rev. Lett **104**, 173601 (2010).
[19] H. Di Lorenzo Pires, C. H. Monken, and M. P. van Exter, Phys. Rev. A **80**, 022307 (2009).
[20] C. K. Law and J. H. Eberly, Phys. Rev. Lett. **92**, 127903 (2004).
[21] L. C. Andrews and R. L. Phillips,*Laser Beam Propagation through Random Media* (SPIE, Bellingham, WA, 2005).